ACS chemical biology

pubs.acs.org/acschemicalbiology

Letters

A Standalone β-Ketoreductase Acts Concomitantly with Biosynthesis of the Antimycin Scaffold

Asif Fazal, Glyn R. Hemsworth,* Michael E. Webb,* and Ryan F. Seipke*

Cite This: *ACS Chem. Biol.* 2021, 16, 1152–1158

Read Online

ACCESS | Metrics & More | Article Recommendations | Supporting Information

ABSTRACT: Antimycins are anticancer compounds produced by a hybrid nonribosomal peptide synthetase/polyketide synthase (NRPS/PKS) pathway. The biosynthesis of these compounds is well characterized, with the exception of the standalone β-ketoreductase enzyme AntM that is proposed to catalyze the reduction of the C8 carbonyl of the antimycin scaffold. Inactivation of *antM* and structural characterization suggested that rather than functioning as a post-PKS tailoring enzyme, AntM acts upon the terminal biosynthetic intermediate while it is tethered to the PKS acyl carrier protein. Mutational analysis identified two amino acid residues (Tyr185 and Phe223) that are proposed to serve as checkpoints controlling substrate access to the AntM active site. Aromatic checkpoint residues are conserved in uncharacterized standalone β-ketoreductases, indicating that they may also act concomitantly with synthesis of the scaffold. These data provide novel mechanistic insights into the functionality of standalone β-ketoreductases and will enable their reprogramming for combinatorial biosynthesis.

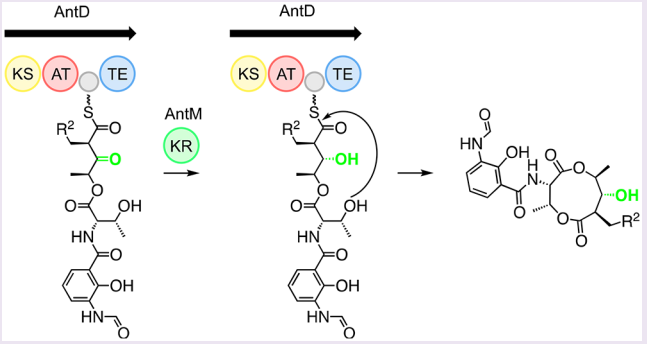

Antimycins (**1**–**4**) are a large family of anticancer compounds produced by several *Streptomyces* species.[1−3] The structures of **1**–**4** consist of a substituted (C7 alkyl, C8 acyloxy, and C4 and C9 methyl) nine-membered dilactone connected to a 3-formamidosalicylamido group at C3 (Figure 1).[4] The hybrid nonribosomal peptide synthetase/polyketide synthase (NRPS/PKS) biosynthetic gene cluster (BGC) responsible for the production of antimycins has been reported,[5] and the proposed biosynthetic pathway is shown in Figure 1.[6−8] A key step in the biosynthesis of antimycin is the reduction of the C8 carbonyl by a standalone β-ketoreductase (KR) named AntM, which is required for the subsequent diversification of the position by AntB, an acyltransferase.[9] Although cis-encoded KR domains within PKSs are well characterized, standalone KRs from assembly-line biosynthetic systems have not been studied in detail.

To investigate the role of AntM in the biosynthesis of antimycins, an in-frame deletion of *antM* on a cosmid clone of the antimycin BGC was constructed and introduced into an antimycin-deficient strain of *S. albidoflavus*. Liquid chromatography−high-resolution mass spectrometry (LC-HRMS) analysis of chemical extracts resulting from this Δ*antM* strain revealed that it no longer produced **1**–**4**, and antimycins harboring a C8 carbonyl or their corresponding unreduced linear intermediates were also not detected (Figure S1). Taken together, these data led to the hypothesis that AntM catalyzes the β-ketoreduction of the C8 carbonyl on the final linear biosynthetic intermediate while it is still covalently attached to $AntD^{ACP}$ and that its activity is required for the ultimate release of the antimycin scaffold *in vivo*.

The hypothesis that AntM may act upon an acyl carrier protein (ACP)-bound intermediate prompted the *in vitro* characterization of the enzyme. AntM was overproduced and purified as an N-terminal hexahistidine fusion protein ($(His)_6$-AntM). The identity of its cognate nicotinamide cofactor was confirmed by screening for the binding of NADPH, $NADP^+$, or NADH using isothermal titration calorimetry (ITC), which showed a 1:1 interaction between AntM and NADPH (6.4 μM) and or $NADP^+$ (19.5 μM) (Figure S2) but no detectable interaction with NADH, confirming that $(His)_6$-AntM is an NADPH-dependent ketoreductase (Figure S2).

To further clarify whether AntM acts upon a linear biosynthetic intermediate, crystal structures were determined for *apo*-AntM (7NM7) and AntM bound to NADPH (7NM8) to 2.1 and 1.7 Å resolution, respectively. The structures are essentially isostructural with very little movement between the two structures, and given that NADPH−AntM represents the active state of the enzyme, all further structural analysis was

Received: March 29, 2021
Accepted: May 12, 2021
Published: June 20, 2021

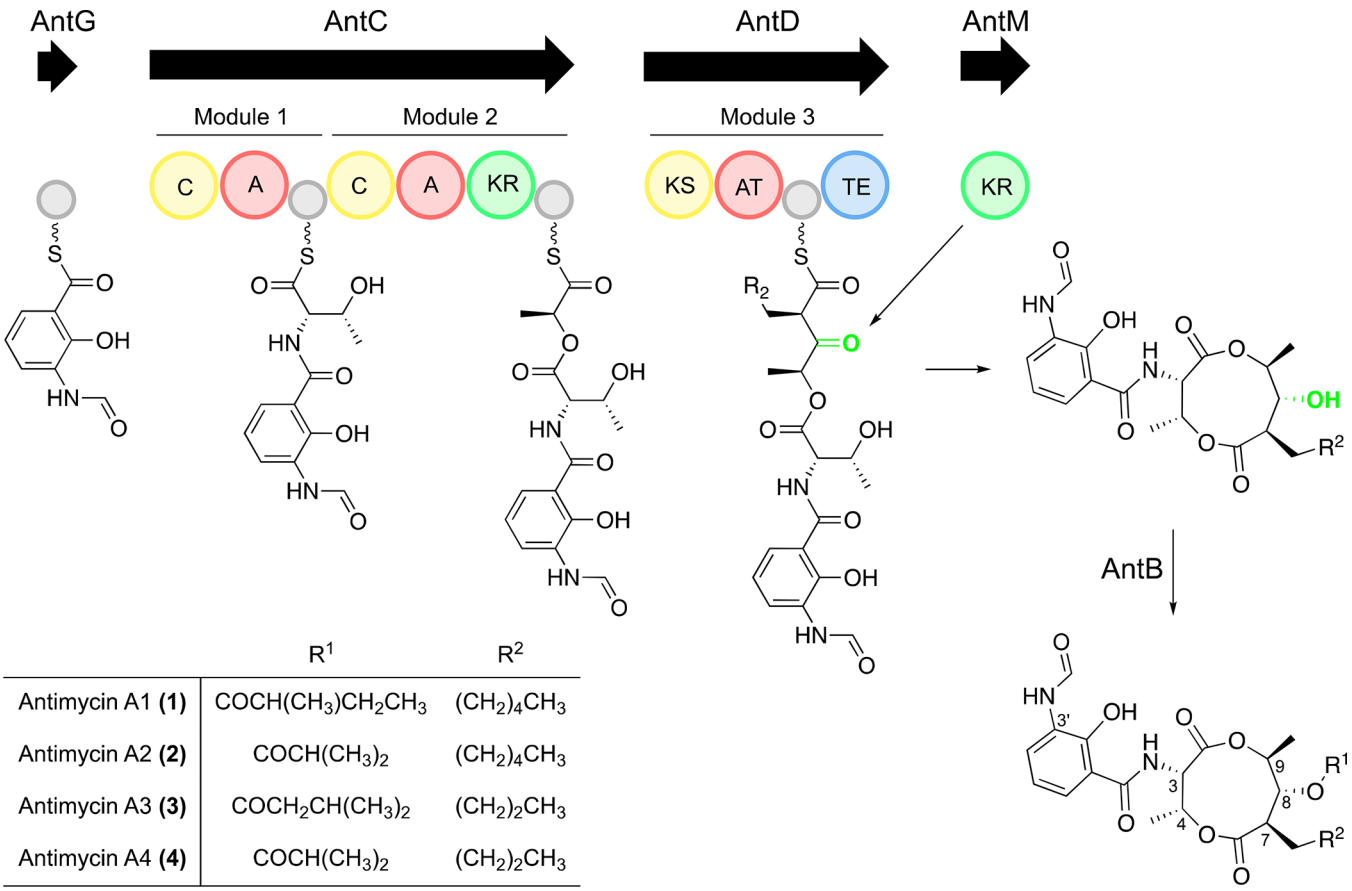

	R^1	R^2
Antimycin A1 **(1)**	$COCH(CH_3)CH_2CH_3$	$(CH_2)_4CH_3$
Antimycin A2 **(2)**	$COCH(CH_3)_2$	$(CH_2)_4CH_3$
Antimycin A3 **(3)**	$COCH_2CH(CH_3)_2$	$(CH_2)_2CH_3$
Antimycin A4 **(4)**	$COCH(CH_3)_2$	$(CH_2)_2CH_3$

Figure 1. Antimycin BGC and proposed biosynthetic pathway. The C8 carbonyl reduced by AntM and the corresponding hydroxyl moiety are green. A, adenylation; C, condensation; KR, ketoreductase; KS, ketosynthase; TE, thioesterase. Small gray circles indicate peptidyl or acyl carrier proteins.

performed using this structure. AntM has a Rossmann-fold architecture typical of the short-chain dehydrogenase/reductase (SDR) enzyme family (InterProID = IPR002347) to which it belongs. As is common for SDRs, AntM was a tetramer that could be constructed around the crystallographic symmetry axis (Figure 2A). The NADPH cofactor is clearly visible within the crystal structure, where it is bound in a pocket by the quintessential NADPH binding motif TGGSRGIG and adjacent to the highly conserved catalytic triad (S178, Y191, K195) typical of SDR family enzymes (Figure 2B).[10] Adjacent to the NADPH cofactor, we also observed some elongated electron density that we were unable to model with confidence (Figure 2B). This may represent a network of water molecules or an elongated molecule such as a PEG fragment from the crystallization solution, but it may also hint that an elongated part of the substrate may bind in this region of the enzyme active site (discussed later).

A comparison of the AntM structure against other structures in the Protein Data Bank (PDB) using PDBeFold[11] revealed its structural similarity to ketoreductases associated with the biosynthesis of tetracyclic aromatic type-II polyketides. The closest structural matches were to the C-terminal domain of UrdM (UrdMred) from *S. fradiae* (4OSP) and LanV from *S. cyanogenus* (4OSO), which are urdamycin and landomycin C6-ketoreductases, respectively (Figure 2C).[12,13] The protomers of these enzymes superpose onto AntM with main-chain root-mean-square deviations (RMSDs) of 0.91 and 0.93 Å, respectively (Figure 2D). These are clearly very similar structures, even though they each share only slightly over 50% amino acid identity with AntM (Figure 2C). The structures of both UrdMred and LanV were determined with an analogue of their product, rabelomycin, bound. This tetracyclic aromatic compound is significantly different from AntM's expected substrate, but Patrikainen et al. used its positioning and the generation of mutants to identify the R1 to R4 regions in UrdMred and LanV, which were important in determining the substrate specificity and regioselectivity. These regions were also recently shown to be important for another tetracyclic aromatic C6-ketoreductase, LugOII (lugdunomycin).[14] Sequence alignment of AntM with UrdMred and LanV proteins shows that the R1−R4 regions around the active site are the regions that diverge most between UrdMred/LanV and AntM (Figure 2C,D), suggesting that these portions of the protein are likely to also determine the substrate specificity of AntM. Interestingly, two of the small side chains that form the rabelomycin binding site in UrdMred (Asn154 and Ile192) and LanV (Ser154 and Ser192) have been replaced by the significantly bulkier side chains of Tyr185 and Phe223 in AntM (Figure 2E). Indeed, these residues fall into the R2 and R3 regions identified by Patrikainen et al., further suggesting that these may be key positions in AntM. Tyr185 occupies a dual conformation in the structure, showing some flexibility in this region, but these differences between the proteins have the effect of converting the substrate binding cleft of UrdMred and LanV into a closed pocket in AntM (Figure 2E). It should also be noted that three residues between Ile228 and Leu232, which form the top face of the substrate binding site in R4, could not be modeled with confidence in the AntM structure, suggesting that there is likely

https://doi.org/10.1021/acschembio.1c00229
ACS Chem. Biol. 2021, 16, 1152−1158

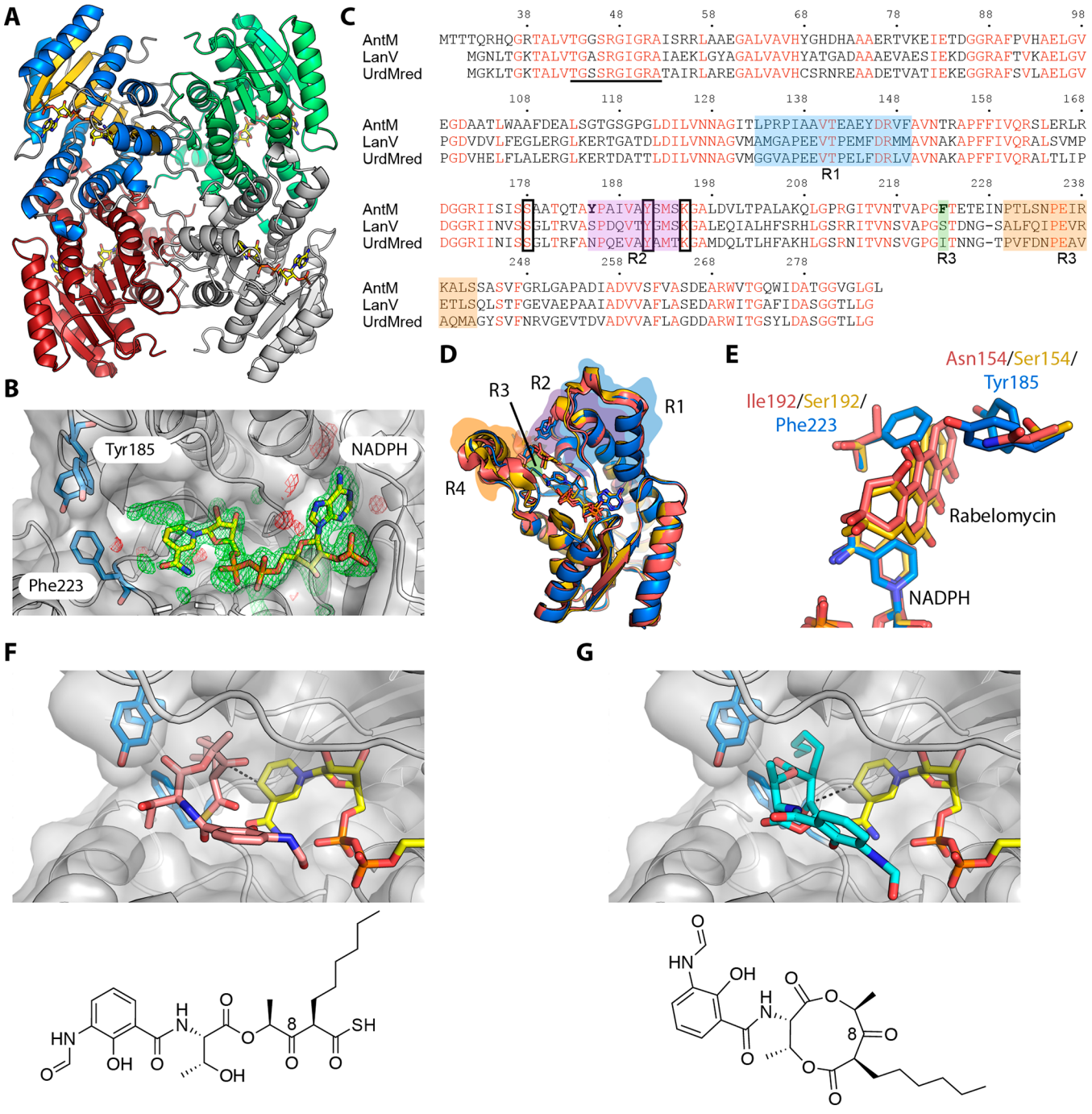

Figure 2. Structural analysis of AntM. (A) AntM tetramer shown as a cartoon and with the protomer present in the asymmetric unit colored by the secondary structure and protomers that are related by crystal symmetry that generate the tetramer colored by the protomer. NADPH is shown as sticks with yellow carbon atoms. (B) View of the enzyme active site showing a polder map generated for the NADPH ligand contoured at 3σ with a 5 Å radius around the NADPH cofactor. Positive density is green, and negative density is red. Unmodeled electron density was observed in a pocket adjacent to the nicotinamide ring of NADPH, which can be observed in the polder map. The protein backbone is shown in the cartoon representation, with the semitransparent protein surface included in gray. (C) Multiple sequence alignment of AntM with LanV and UrdMred. The NADPH binding residues are highlighted by the black line and catalytic triad by black boxes. The R1, R2, R3 and R4 regions are highlighted by blue, violet, green and orange boxes, respectively. Phe223 and Tyr185 residues from AntM are in bold text. (D) Overall superposition of AntM (blue) with UrdMred (pink) and LanV (yellow), showing their structural similarity. Regions R1−R4 are highlighted in the same colors used for panel C. (E) Close-up view in the active site when AntM (blue), UrdMred (pink), and LanV (yellow) are superposed. The rabelomycin from UrdMred and LanV structures would clash with Phe223 and Tyr185, suggesting that these residues mediate an important change in the active site architecture that may determine AntM's substrate specificity. (F) Third best binding pose for the linear substrate (pink). (G) Third best binding pose for the cyclized substrate (cyan). In both panels, the AntM residues selected for mutation in activity studies are shown with blue carbon atoms, and NADPH is shown with yellow carbon atoms. The distances between the reducing face of the NADPH and the C8 of substrates to be reduced are shown by black dashed lines.

flexibility in this region that may also influence how the enzyme interacts with its substrate. These residues could become more ordered upon binding to substrate, but without a ligand complex structure for AntM, this possibility cannot be examined. Finally,

https://doi.org/10.1021/acschembio.1c00229
ACS Chem. Biol. 2021, 16, 1152−1158

outside of the R1−R4 region and further down the likely substrate binding cleft, Met101 in UrdMred/LanV is replaced with Thr132 in AntM, enabling the possibility for substrates to also bind in this region, potentially in an extended conformation. These structural differences suggested that AntM may therefore bind its substrate significantly differently from UrdMred/LanV.

Molecular docking was used to investigate potential modes for substrate binding to AntM. Asn229, Pro230, and Thr231 which could not be modeled based on the observed electron density, were manually modeled for this analysis. This provided a more complete model of the active site as a starting point for the docking analysis. Binding to the AntM structure was investigated for the linear and cyclized peptide intermediates. A range of binding poses were observed for both substrates (Figures S3). In all of the docking poses for the linear substrate and for several docking poses of the product, the R^2 acyl chain was observed to occupy a pocket adjacent to the NADPH headgroup formed by Tyr185 and occupied by the unmodeled electron density previously discussed. This suggests that this region could be important for optimal positioning of the substrate for catalysis. In addition, the binding pose in which the *Si* face of the substrate carbonyl to be reduced (C8) most closely approaches NADPH was observed in the linear substrate at only 4.2 Å (Figure 2F). The binding poses for the cyclized substrate were far more diverse, although a binding pose in which the incorrect *Re* face of the C8 carbonyl is 4.3 Å from the NADPH was observed (Figure 2G). Overall, these docking studies indicate that AntM most likely acts upon the linear biosynthetic intermediate and that the positioning of the R^2 acyl chain may be an important determinant of the substrate specificity. Given their importance in forming the R^2 pocket, the docking analysis also lends further support to Tyr185 and Phe223 playing a key role in constructing the appropriate active-site geometry for the enzyme to act on its substrate.

Analysis of the AntM structure suggested that Tyr185 and Phe223 may be key residues that control access to the substrate binding pocket. The importance of these positions was investigated by substituting Tyr185 and Phe223 with either Trp or Ala. Substitution with Trp was predicted to abrogate activity by occluding binding of the linear but not the cyclized substrate, whereas substitution with Ala was predicted to open up the pocket without severely affecting the activity. Thus four variants, AntM^{Y185W}, AntM^{F223W}, AntM$^{Y185W-F223W}$, and AntM$^{Y185A-F223A}$, were generated and used to genetically complement the Δ*antM* gene deletion to evaluate the importance of these positions. In line with our hypothesis, LC-HRMS analysis of the resulting strains indicated that complementation with the Y185A−F223A variant resulted in antimycin production levels comparable to those of complementation with wild-type *antM*, whereas production was severely compromised for strains complemented with Y185W, F223W, or Y185W−F223W (Figure 3). To ensure that the observed phenotypes were not due to compromised cofactor binding, ITC was used with $(His)_6$-AntM^{Y185W}, $(His)_6$-AntM^{F223W}, and $(His)_6$-AntM$^{Y185W-F223W}$ to confirm NADPH binding had not been disrupted. This experiment revealed that the mutant variants all bound to NADPH equally well as the wild-type protein, with K_D values in the micromolar range (Figure S2). Overall, these data strongly support the structural analysis and further indicate that these residues are important for the correct positioning of an ACP-bound linear substrate within the active site to allow antimycin maturation.

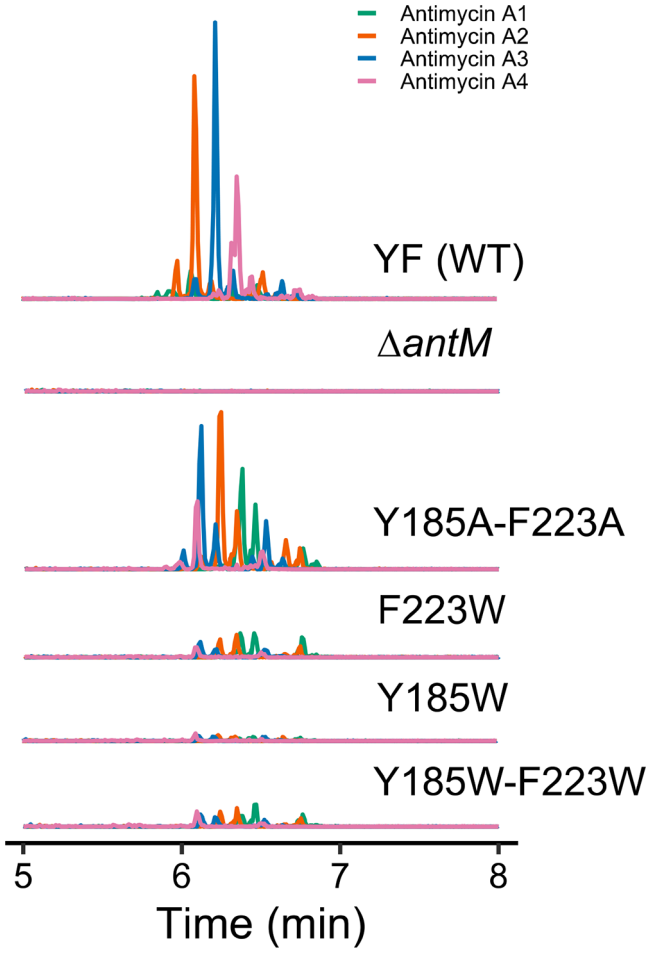

Figure 3. Tyr185 and Phe223 are important for AntM function and antimycin production. LC-HRMS analysis of chemical extracts prepared from the Δ*antM* strain complemented with the indicated variants of *antM*. The *m*/*z* values corresponding to the $[M + H]^+$ and $[M + Na]^+$ ions derived from **1**−**4** are shown and are color-coded as indicated. The intensity scale for each extracted-ion chromatogram (EIC) is the same, with a maximum value of 2.5×10^5.

Whereas it is established that some KRs from type-II PKS systems can act upon ACP-bound intermediates,[15] the data presented here are the first to indicate that a standalone KR acts upon a linear biosynthetic intermediate tethered to a type-I PKS assembly line. To evaluate how widespread KRs like AntM may be and to understand their relationship to other KRs, a phylogenetic analysis was performed using KRs from the MIBiG repository.[16] An inspection of the resulting phylogeny indicated that AntM is more closely related to standalone KRs from type-II PKS systems than cis-encoded KRs. This observation is consistent with its structural similarity to UrdMred/LanV (Table S1, Figure 4) and suggests that standalone KRs from assembly-line systems may be co-opted from type-II PKS BGCs as opposed to being derived from excised KR domains from type-I PKSs. Interestingly, an inspection of the multiple sequence alignment for these KRs revealed that 17 of them harbored an aromatic amino acid residue in at least one of the positions identified as important for AntM activity in this study (Figure 4). Of these 17, 7 originate from type-II PKS systems, and 3 of them have been biochemically characterized. FdmC (fredericamycin) and SanC (A-74528) perform a ketoreduction of the final ACP-bound acyl chain for elongation, and StfT

https://doi.org/10.1021/acschembio.1c00229
ACS Chem. Biol. 2021, 16, 1152−1158

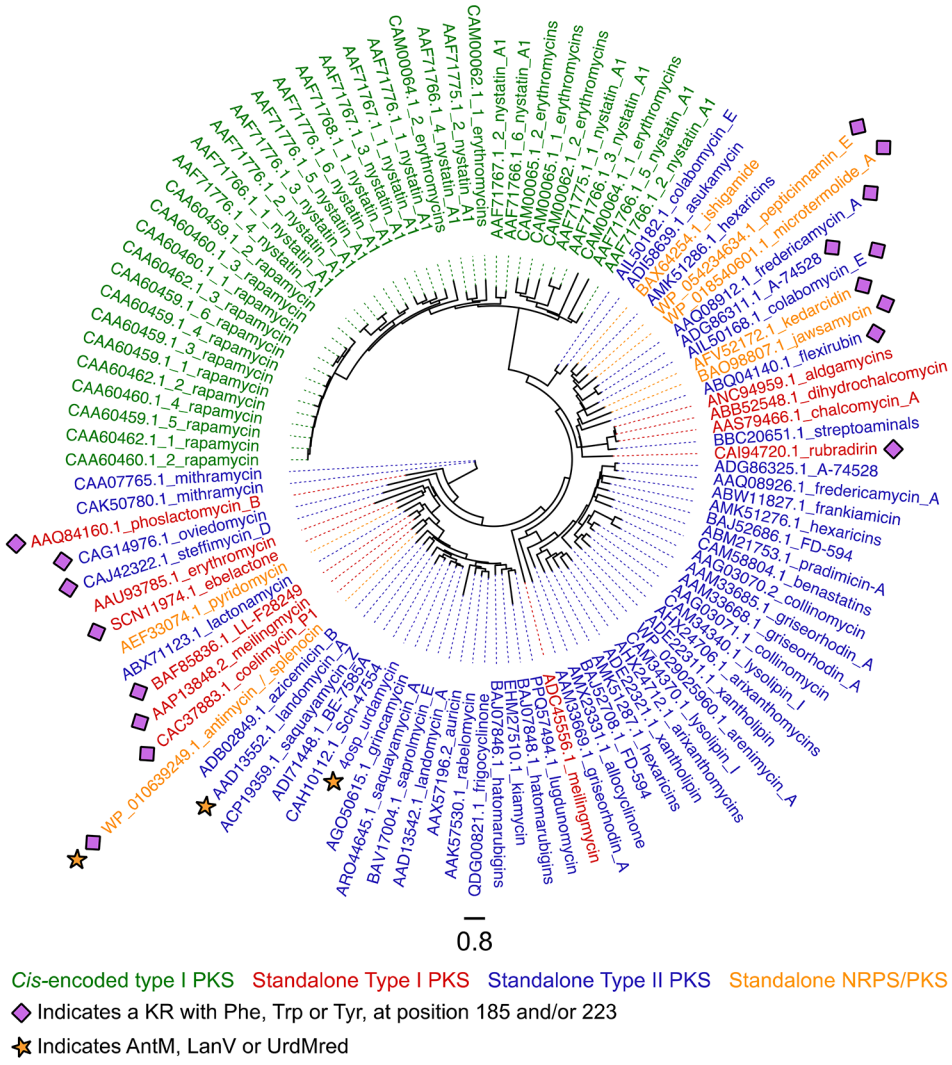

Protein accession	Biosynthetic system	Product	-1	AntM Y185	+1	-1	AntM F223	+1
AAP13848.2	Standalone Type I PKS	Meilingmycin	A	W	P	G	I	T
AAQ08912.1	Standalone Type II PKS	Fredericamycin A	G	N	A	G	F	I
AAQ84160.1	Standalone Type I PKS	Phoslactomycin B	A	Y	P	G	L	I
ABQ04140.1	Standalone Type II PKS	Flexirubin	G	T	A	G	F	I
ADG86311.1	Standalone Type II PKS	A-74528	G	N	P	G	F	I
AFV52172.1	Standalone Hybrid NRPS/PKS	Kedarcidin	G	N	A	G	F	I
AIL50168.1	Standalone Type II PKS	Colabomycin E	G	N	A	G	F	I
BAF85836.1	Standalone Type I PKS	LL-F28249	A	W	P	G	I	T
BAJ07848.1	Standalone Type II PKS	Hatomarubigins	A	F	P	G	I	T
BAO98807.1	Standalone Hybrid NRPS/PKS	Jawsamycin	G	A	P	G	F	I
CAC37883.1	Standalone Type I PKS	Coelimycin P1	A	F	P	G	T	I
CAG14976.1	Standalone Type II PKS	Oviedomycin	T	A	P	G	F	V
CAI94720.1	Standalone Type I PKS	Rubradirin	G	N	P	G	Y	V
CAJ42322.1	Standalone Type II PKS	Steffimycin D	A	W	P	G	V	I
SCN11974.1	Standalone Type I PKS	Ebelactone	A	F	P	G	P	I
WP_010639249.1	Standalone Hybrid NRPS/PKS	Antimycin / splenocin	A	Y	P	G	F	T
WP_018540601.1	Standalone Hybrid NRPS/PKS	Microtermolide A	G	N	S	G	F	V
WP_054234634.1	Standalone Hybrid NRPS/PKS	Pepticinnamin E	G	H	A	G	Y	I

Figure 4. Bioinformatics analysis of KR sequences. The upper panel shows an approximate maximum-likelihood phylogenetic tree composed of 107 KR sequences. The scale bar represents 0.8 substitutions per site. The lower panel shows KRs with aromatic amino acid residues at positions 185 and/or 223. Positions 184 and 222 are indicated by −1, and positions 186 and 224 are indicated by +1.

(steffimycin) performs a ketoreduction on an offloaded partially cyclized intermediate.[17−19] Ten of the remaining 17 KRs are from either type-I PKS or NRPS/PKS systems and are not experimentally characterized. Interestingly, the 17 KRs with aromatic residues in the positions identified here cluster within two distinct groups in the tree (Figure 4). It is an attractive hypothesis to suggest that those grouped with AntM may also act upon ACP-bound intermediates.

https://doi.org/10.1021/acschembio.1c00229
ACS Chem. Biol. 2021, 16, 1152−1158

In summary, AntM has been extensively characterized as a standalone β-ketoreductase that reduces the C8 carbonyl of the linear terminal biosynthetic intermediate in antimycin production while it remains tethered to AntD^{ACP}. Although this is the first characterization of a standalone KR acting concomitantly with a type-I PKS assembly line, bioinformatics analyses suggest that AntM is unlikely to be unique in this respect. AntM has joined a growing list of standalone enzymes that do not perform post-assembly-line tailoring functions but rather act concomitantly with biosynthesis. The major challenge ahead is to provide molecular insight into the protein−protein contacts that are presumably required for facilitating an interaction with assembly-line-like biosynthetic systems so that these standalone enzymes can be effectively reprogrammed for combinatorial biosynthesis.

■ ASSOCIATED CONTENT

Supporting Information

The Supporting Information is available free of charge at https://pubs.acs.org/doi/10.1021/acschembio.1c00229.

Experimental procedures. Figure S1. LC-HRMS of wild-type (WT) Δ*antM* strains. Figure S2. ITC analysis of AntM proteins binding to nicotinamide cofactors. Figure S3. Docking analyses of substrates into AntM. Table S2. Bacterial strains, cosmids, plasmids, and oligos used in this study. Table S3. AntM structure data collection and refinement statistics (PDF)

Table S1. KRs analyzed in this study (XLSX)

Accession Codes

The atomic coordinates of AntM structures have been deposited in the Protein Data Bank (PDB IDs: 7NM7 and 7NM8).

■ AUTHOR INFORMATION

Corresponding Authors

Glyn R. Hemsworth − *Astbury Centre for Structural Molecular Biology, University of Leeds, Leeds LS2 9JT, United Kingdom; Faculty of Biological Sciences, University of Leeds, Leeds LS2 9JT, United Kingdom;* orcid.org/0000-0002-8226-1380; Email: g.r.hemsworth@leeds.ac.uk

Michael E. Webb − *Astbury Centre for Structural Molecular Biology, University of Leeds, Leeds LS2 9JT, United Kingdom; School of Chemistry, University of Leeds, Leeds LS2 9JT, United Kingdom;* orcid.org/0000-0003-3574-4686; Email: m.e.webb@leeds.ac.uk

Ryan F. Seipke − *Astbury Centre for Structural Molecular Biology, University of Leeds, Leeds LS2 9JT, United Kingdom; Faculty of Biological Sciences, University of Leeds, Leeds LS2 9JT, United Kingdom;* orcid.org/0000-0002-6156-8498; Email: r.seipke@leeds.ac.uk

Author

Asif Fazal − *Astbury Centre for Structural Molecular Biology, University of Leeds, Leeds LS2 9JT, United Kingdom; Faculty of Biological Sciences and School of Chemistry, University of Leeds, Leeds LS2 9JT, United Kingdom*

Complete contact information is available at: https://pubs.acs.org/10.1021/acschembio.1c00229

Author Contributions

Conceptualization: A.F., M.E.W., and R.F.S.; Investigation: A.F. and R.F.S.; Formal Analysis: G.R.H.; Writing, Original Draft: A.F., G.R.H., and R.F.S.; Writing, Review and Editing: A.F., G.R.H., M.E.W., and R.F.S.; Funding acquisition: M.E.W. and R.F.S.; Project Administration: R.F.S.

Notes

The authors declare no competing financial interest.

■ ACKNOWLEDGMENTS

This work was carried out with the support of Diamond Light Source, Beamline i04 (proposal MX19248). We thank I. Manfield for the assistance with ITC. A.F. was supported by a University of Leeds Ph.D. studentship. G.R.H. was supported by BBSRC David Phillips Fellowship BB/N019970/1. R.F.S. and M.E.W. were supported by BBSRC responsive mode grant BB/T008075/1.

■ REFERENCES

(1) Joynt, R., and Seipke, R. F. (2018) A phylogenetic and evolutionary analysis of antimycin biosynthesis. *Microbiology 164*, 28−39.

(2) Liu, J., Zhu, X., Kim, S. J., and Zhang, W. (2016) Antimycin-type depsipeptides: discovery, biosynthesis, chemical synthesis, and bioactivities. *Nat. Prod. Rep. 33*, 1146−1165.

(3) Schwartz, P. S., Manion, M. K., Emerson, C. B., Fry, J. S., Schulz, C. M., Sweet, I. R., and Hockenbery, D. M. (2007) 2-Methoxy antimycin reveals a unique mechanism for Bcl-x $_L$ inhibition. *Mol. Cancer Ther. 6*, 2073−2080.

(4) van Tamelen, E. E., Dickie, J. P., Loomans, M. E., Dewey, R. S., and Strong, F. M. (1961) The chemistry of antimycin A. X. Structure of the antimycins. *J. Am. Chem. Soc. 83*, 1639−1646.

(5) Seipke, R. F., Barke, J., Brearley, C., Hill, L., Yu, D. W., Goss, R. J. M., and Hutchings, M. I. (2011) A single *Streptomyces* symbiont makes multiple antifungals to support the fungus farming ant *Acromyrmex octospinosus*. *PLoS One 6*, No. e22028.

(6) Sandy, M., Rui, Z., Gallagher, J., and Zhang, W. (2012) Enzymatic synthesis of dilactone scaffold of antimycins. *ACS Chem. Biol. 7*, 1956−1961.

(7) Schoenian, I., Paetz, C., Dickschat, J. S., Aigle, B., Leblond, P., and Spiteller, D. (2012) An unprecedented 1,2-shift in the biosynthesis of the 3-aminosalicylate moiety of antimycins. *ChemBioChem 13*, 769−773.

(8) Yan, Y., Zhang, L., Ito, T., Qu, X., Asakawa, Y., Awakawa, T., Abe, I., and Liu, W. (2012) Biosynthetic pathway for high structural diversity of a common dilactone core in antimycin production. *Org. Lett. 14*, 4142−4145.

(9) Sandy, M., Zhu, X., Rui, Z., and Zhang, W. (2013) Characterization of AntB, a promiscuous acyltransferase involved in antimycin biosynthesis. *Org. Lett. 15*, 3396−3399.

(10) Filling, C., Berndt, K. D., Benach, J., Knapp, S., Prozorovski, T., Nordling, E., Ladenstein, R., Jörnvall, H., and Oppermann, U. (2002) Critical Residues for structure and catalysis in short-chain dehydrogenases/reductases. *J. Biol. Chem. 277*, 25677−25684.

(11) Krissinel, E., and Henrick, K. (2004) Secondary-structure matching (SSM), a new tool for fast protein structure alignment in three dimensions. *Acta Crystallogr., Sect. D: Biol. Crystallogr. 60*, 2256−2268.

(12) Paananen, P., Patrikainen, P., Kallio, P., Mantsala, P., Niemi, J., Niiranen, L., and Metsa-Ketela, M. (2013) Structural and functional analysis of angucycline C-6 ketoreductase LanV involved in landomycin biosynthesis. *Biochemistry 52*, 5304−5314.

(13) Patrikainen, P., Niiranen, L., Thapa, K., Paananen, P., Tähtinen, P., Mäntsälä, P., Niemi, J., and Metsä-Ketelä, M. (2014) Structure-based engineering of angucyclinone 6-ketoreductases. *Chem. Biol. 21*, 1381−1391.

(14) Xiao, X., Elsayed, S. S., Wu, C., van der Heul, H. U., Metsä-Ketelä, M., Du, C., Prota, A. E., Chen, C.-C., Liu, W., Guo, R.-T., et al. (2020) Functional and structural insights into a novel promiscuous ketoreductase of the lugdunomycin biosynthetic pathway. *ACS Chem. Biol. 15*, 2529−2538.

(15) Hertweck, C., Luzhetskyy, A., Rebets, Y., and Bechthold, A. (2007) Type II polyketide synthases: gaining a deeper insight into enzymatic teamwork. *Nat. Prod. Rep. 24*, 162−190.
(16) Medema, M. H., Kottmann, R., Yilmaz, P., Cummings, M., Biggins, J. B., Blin, K., de Bruijn, I., Chooi, Y. H., Claesen, J., Coates, R. C., et al. (2015) Minimum Information about a biosynthetic gene cluster. *Nat. Chem. Biol. 11*, 625−631.
(17) Das, A., Szu, P.-H., Fitzgerald, J. T., and Khosla, C. (2010) Mechanism and engineering of polyketide chain initiation in fredericamycin biosynthesis. *J. Am. Chem. Soc. 132*, 8831−8833.
(18) Wang, G., Chen, J., Zhu, H., and Rohr, J. (2017) One-Pot enzymatic total synthesis of presteffimycinone, an early intermediate of the anthracycline antibiotic steffimycin Biosynthesis. *Org. Lett. 19*, 540−543.
(19) Zaleta-Rivera, K., Charkoudian, L. K., Ridley, C. P., and Khosla, C. (2010) Cloning, sequencing, heterologous expression, and mechanistic analysis of A-74528 biosynthesis. *J. Am. Chem. Soc. 132*, 9122−9128.

https://doi.org/10.1021/acschembio.1c00229
ACS Chem. Biol. 2021, 16, 1152−1158